Iron Normal Mode Dynamics in (Nitrosyl)iron(II)tetraphenylporphyrin from X-ray Nuclear Resonance Data

Brajesh K. Rai,* Stephen M. Durbin,* Earl W. Prohofsky,* J. Timothy Sage,[†] Graeme R. A. Wyllie,[‡] W. Robert Scheidt,[‡] Wolfgang Sturhahn,[§] and E. Ercan Alp[§]

*Department of Physics, Purdue University, West Lafayette, Indiana 47907, [†]Department of Physics, Northeastern University, Boston, Massachusetts 02115, [‡]Department of Chemistry and Biochemistry, University of Notre Dame, Notre Dame, Indiana, 46556, and [§]Advanced Photon Source, Argonne National Laboratory, Argonne, Illinois 60439 USA

ABSTRACT   The complete iron atom vibrational spectrum has been obtained by refinement of normal mode calculations to nuclear inelastic x-ray absorption data from (nitrosyl)iron(II)tetraphenylporphyrin, FeTPP(NO), a useful model for heme dynamics in myoglobin and other heme proteins. Nuclear resonance vibrational spectroscopy (NRVS) provides a direct measurement of the frequency and iron amplitude for all normal modes involving significant displacement of ^{57}Fe. The NRVS measurements on isotopically enriched single crystals permit determination of heme in-plane and out-of-plane modes. Excellent agreement between the calculated and experimental values of frequency and iron amplitude for each mode is achieved by a force-field refinement. Significantly, we find that the presence of the phenyl groups and the NO ligand leads to substantial mixing of the porphyrin core modes. This first picture of the entire iron vibrational density of states for a porphyrin compound provides an improved model for the role of iron atom dynamics in the biological functioning of heme proteins.

INTRODUCTION

Nuclear resonance vibrational spectroscopy (NRVS) is a new spectroscopic tool for the study of dynamics of Mössbauer nuclei in a wide range of materials (Seto et al., 1995; Sturhahn et al., 1995; Keppler et al., 1997; Toellner et al., 1997; Chumakov and Rüffer, 1998). The availability of high brightness radiation from third-generation synchrotron sources and the development of x-ray monochromators with sub-meV energy resolution have allowed the development of this technique to study vibrational dynamics. Conventional Mössbauer spectroscopy measures the total mean square displacement (m.s.d.) of a Mössbauer nucleus, an average over all normal mode frequencies. In contrast, NRVS can be used to observe amplitudes and frequencies of the individual vibrational modes involving motion of the Mössbauer nucleus without the optical selection rules that limit similar spectra obtained from Raman scattering. NRVS is well suited for studying the dynamics of iron atoms in large biological macromolecules containing heme molecules, and heme model compounds. NRVS has been recently applied to study the iron dynamics of an ^{57}Fe-enriched heme protein, myoglobin (Parak and Achterhold, 1999; Keppler et al., 2000; Sage et al., 2001a).

We report here on the iron dynamics of the heme compound (nitrosyl)iron(II)tetraphenylporphyrin, FeTPP(NO). This compound provides a useful model for heme proteins having fivefold coordinated iron atoms. Metalloporphyrins have long been the subject of intensive research to gain insight into heme protein behavior (Spiro and Li, 1988; Li et al., 1989, 1990a, b; Choi et al., 1991; Procyk and Bocian, 1992; Lipscomb et al., 1993; Rush et al., 2000; Kincaid, 2000). Porphyrin compounds with 4-coordinated, 5-coordinated, and 6-coordinated forms have been extensively studied using Resonance Raman (RR) and infrared (IR) techniques. The porphyrin complex gives rise to strongly allowed electronic transitions in the visible and ultraviolet region, which couple to vibrational modes to give richly detailed resonance Raman spectra. Several vibrational modes in the region of 1200–1600 cm^{-1}, for example, depend strongly upon the detailed structure of the porphyrin ring and the oxidation, spin, and ligand-coordination state of the central metal ion (Spiro and Li, 1988; Kincaid, 2000).

The task of determining which atoms contribute to a particular Raman line is often aided by selective isotopic substitution. However, the technique can yield ambiguous results for low-frequency modes, because these modes tend to be delocalized, i.e., the potential energy distribution (PED) of these modes contains contributions from many internal coordinates and involves the motion of a relatively large number of atoms. In addition, the RR and IR optical selection rules do not allow observation of the majority of the vibrational modes involving iron motion, which further limits the capability of optical spectroscopies. A significant advantage of NRVS is that optical selection rules do not apply. Any normal mode that has significant amplitude of iron motion (in the direction of the incident x-ray photon) can be observed. The NRVS not only indicates the frequencies of Fe modes unambiguously, but also quantitatively determines the iron amplitudes in each mode. In contrast, fits to RR data primarily concern the frequencies of the modes, because it can be difficult to model the intensity of

RR lines due to various uncertainties in the matrix elements for the electron–phonon interaction. As a result, the fitting of normal-mode calculations to NRVS data is significantly more constrained than it would be with RR data, giving greater confidence in the reliability of the final results.

In this paper, we extend NRVS to single-crystal samples. Initial data on polycrystalline FeTPP(NO) provide an isotropically-averaged vibrational density of states (Sage et al., 2001b). We subsequently repeated the NRVS measurements with the incident x-ray beam nearly parallel to the porphyrin planes of a set of small, oriented single crystals. This geometry suppresses the out-of-plane modes, because here the iron motion is largely perpendicular to the incident beam. Comparison of polycrystalline and oriented crystal data provides an experimental determination of the in-plane versus out-of-plane character of many modes, an important constraint on the fitting process.

We describe below the normal mode analysis formalism and NRVS technique and show how iron vibrational density of states (VDOS) can be calculated from the normal mode analysis. We refine our initial set of force fields to get an acceptable match for the calculated VDOS with the experimental data. Results from the normal mode analysis with the refined set of force constants are used to assign experimental modes using the modes of the bare heme molecule as a basis set. Several porphyrin in-plane modes, such as v_{42}, v_{50}, and v_{53}, have been positively identified for the first time, because they are Raman-inactive vibrations. We also identify the nitrosyl ligand stretch and bending modes, and observe the ligand's effect on various porphyrin modes. At frequencies below 150 cm^{-1}, the iron VDOS is dominated by out-of-plane porphyrin modes, modes due to collective motion of the peripheral phenyl rings, and acoustic modes. Modes at 74 and 128 cm^{-1} involve strong coupling between ligand vibrations and the delocalized motion of the porphyrin core. The 74 cm^{-1} mode exhibits a doming-like motion (symmetry type γ_9) of the porphyrin core. The character of the mode at 128 cm^{-1} is defined by pyrrole tilting motion, which opposes the out-of-plane displacement of iron; this mode is identified to be of symmetry type γ_6. In a heme protein, these modes may provide a channel for communicating the ligand state to the protein side chains.

METHODS

Sample preparation

A polycrystalline powder sample of ^{57}FeTPP(NO) was prepared using a modification of the previously reported procedure (Scheidt and Frisse, 1975). Isotopically enriched ^{57}FeTPP(Cl) was prepared according to a previously reported synthesis (Landergren and Baltzer, 1990). Fifty milligrams of this complex was weighed into a Schlenk flask, evacuated, and refilled with argon. Five milliliters chloroform, 1 mL methanol, and 0.5 mL pyridine were added, and the solution degassed several times. Purified nitric oxide was then bubbled through the solution for ~5 min. The product, FeTPP(NO), was precipitated by addition of ~40 mL methanol. The dark purple powder was collected on sintered glass and dried by means

of an aspirator setup. Thirty-five milligrams of this product was then mixed with a small amount of Apiezon M grease to form a thick, dark mull, which was used to fill the sample holder.

Single crystals of ^{57}FeTPP(NO) were prepared using a modification of the technique previously described. Twenty-five milligrams ^{57}FeTPP(Cl) was weighed into a 10-mL beaker. The beaker was placed in a crystallization jar, stoppered, evacuated, then refilled with argon. 2.5 mL chloroform, 0.5 mL methanol, and 2 drops pyridine were added to the beaker via cannula while 4 mL of a 90/10 mixture of chloroform/methanol was added to the outside of the beaker. Purified nitric oxide was bubbled through the crystallization jar, initially through the nonsolvent mixture then through the reaction mixture for ~5 min each. The jar was then sealed, and crystals were allowed to grow by vapor diffusion over a period of 18 days. After this time, tetragonal bipyramidal crystals of approximate dimensions $0.23 \times 0.23 \times 0.18$ mm were harvested. A 5×5 assembly of tetragonal bipyramidal crystals with the porphyrin plane parallel to the sample holder base was then constructed by embedding the crystals in a thin layer of silicon grease. A prior single-crystal x-ray diffraction study of FeTPP(NO) (Scheidt and Frisse, 1975), had shown that the porphyrin plane of the molecule is orientated parallel to the basal plane of the tetragonal bipyramidal crystals. We estimate that the basal planes of these crystals were parallel within a few degrees.

Nuclear resonance vibrational spectroscopy

The ^{57}Fe nuclear Mössbauer resonance at 14.413 keV is used to explore iron vibrational dynamics by measuring the absorption spectrum of x-rays within the range of vibrational energies about the resonance. The techniques for NRVS have been described elsewhere (Seto et al., 1995; Sturhahn et al., 1995; Keppler et al., 1997; Chumakov and Sturhahn, 1999). The measurements discussed here were conducted at sector 3-ID of the Synchrotron Radiation Instrumentation–Collaborative Access Team at the Advanced Photon Source, Argonne National Laboratory, where the incident beam is conditioned first by a diamond premonochromator and then by a dispersive pair of asymmetric (975) silicon crystals for a final energy resolution of 0.85 meV (~7 cm^{-1}) and a photon flux of ~1 GHz (Toellner et al., 1997). Time-delayed iron atomic potassium fluorescence was monitored to determine the rate of resonant nuclear excitation, which is a function of the density of vibrational excitations whose energy matches the difference between the x-ray and nuclear resonance energies. Specimens were mounted on a helium-flow cryostat to permit low temperature measurements. Absorption data were converted to the Fe VDOS using the PHOENIX algorithm of Sturhahn (Sturhahn et al., 1995; Sturhahn and Kohn, 1999; Sturhahn, 2000).

Normal mode analysis

Normal mode calculations on FeTPP(NO) model consisting of 79 atoms were performed in a mass-weighted Cartesian coordinate system. The 20 phenyl ring and 8 beta hydrogen atoms were explicitly included in the calculation. The structural parameters of the FeTPP(NO) model used in the calculations are shown in the Table 1, and the structure of this compound is shown in Fig. 1 (Rush et al., 2000; Scheidt et al., 2000). The four pyrrole rings were set to be coplanar and the phenyl rings were oriented to be perpendicular to the plane defined by the four pyrrole nitrogens. X-ray analysis has shown that this compound can exist in several slightly different conformations, with ruffled or saddled porphyrin cores, or with slightly tilted phenyl rings (Scheidt et al., 2000). Lacking precise structural characterization of our specimens, we assume that the molecules have the ideal planar form for the porphyrin core. These structural parameters are listed in Table 1. We found little change in the calculated normal-mode spectrum when these modifications were explicitly included. The effects of such structural differences should show up in the final refined force fields. We position the iron atom to be 0.3 Å above the mean plane of the pyrrole

TABLE 1 Structural parameters used in the normal-mode calculation (Rush et al., 2000; Scheidt et al., 2000)

	Bond length (Å)		Bond angle (deg.)
C_t-Fe	0.30	Fe-N_L-O	149.0
Fe-N_L	1.69	N_P-C_t-N_P	90.0
N_L-O	1.14	C_α-N_P-C_t	127.6
C_t-N_P	2.01	C_α-N_P-C_α	104.8
C_α-N_P	1.38	C_β-C_α-N_P	110.7
C_α-C_β	1.44	C_β-C_β-C_α	106.7
C_β-C_β	1.35	C_α-C_β-H_β	128.0
C_β-H_β	1.09	C_β-C_β-H_β	125.3
C_α-C_m	1.43	N_P-C_α-C_m	127.1
C_m-C_P	1.51	C_β-C_α-C_m	122.2
C_P-C_P	1.38	C_α-C_m-C_α	120.2
C_P-H_P	1.09	C_α-C_m-C_1	119.9
		C_m-C_1-C_P	120.0
		C_P-C_P-C_P	120.0
		C_P-C_P-H_P	120.0

All the pyrrole atoms (except iron) lie in one plane. C_t indicates the center of the porphyrin core. The iron atom lies 0.3 Å above the center of the heme plane. The Fe-N_L bond makes an angle of 6° from the heme normal. The projection of the FeN_L O bond onto the porphyrin plane makes an angle of 40° from the closest Fe-$N_{P,I}$ vector.

rings, consistent with previous structure determination (Scheidt et al., 2000). The FeN_L vector makes an angle of ~6° from the heme normal, and the FeN_LO angle was set to be 149°. (We denote the nitrosyl ligand nitrogen atom as N_L, as opposed to the pyrrole nitrogens, N_P.) The FeN_LO plane makes an angle of 40° from the closest FeN_P bond. The initial set of force constants were transferred from the earlier works of Li et al. (1989) and Rush et al. (2000), who considered a nickel analog of this porphyrin. The potential energy of the system was expressed using Wilson-type force fields (Wilson et al., 1955). The diagonal elements of the force constant matrix correspond to the stretch, angle bend, torsion, and out-of-plane bending force constants. In addition, off-diagonal terms, corresponding to interactions between diagonal force constants, were also included.
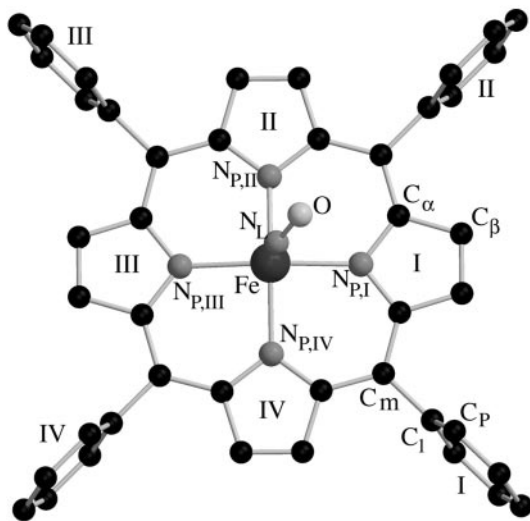

FIGURE 1 Structure of the model FeTPP(NO). For clarity, the beta hydrogens and the hydrogen atoms on the phenyl rings have been omitted.

In the mass-weighted Cartesian coordinate system, the kinetic energy matrix is diagonal and unity. The secular equation describing the vibrational dynamics of the system is

$$[B^\dagger FB - \omega^2 I] = 0, \qquad (1)$$

where F is a square matrix of order m (the number of internal coordinates), which describes the force constants in internal coordinates. B is the transformation matrix (order m by $3n$, where $3n$ is the total number of degrees of freedom in the system) that projects the internal coordinates onto the mass-weighted Cartesian displacement coordinates. Solving the secular equation results in $3n - 6$ nonzero eigenvalues (ω_i^2), which are the squared frequencies of the normal modes. The $3n$-dimensional vector ($\mathbf{Q}_i$) describing the normal coordinates for the ith mode can be linearly transformed to give the mass-weighted Cartesian displacements (q_i) for each atom in that mode by the equation (Cyvin, 1968),

$$\mathbf{q}_i = \sqrt{\frac{h}{8\pi^2 c\omega_i} \coth \frac{hc\omega_i}{2kT}} \, \mathbf{Q}_i, \qquad (2)$$

where c is the speed of light, k is Boltzmann's constant, and T the absolute temperature. To calculate the inelastic x-ray nuclear resonant absorption probability or the iron VDOS for comparison with the NRVS results, only a projection of the $3N$ dimensional vector ($\mathbf{q}_i$) onto a three-dimensional subspace describing the displacement of the iron nucleus ($\boldsymbol{\mu} = q_{i,Fe}/\sqrt{m_{Fe}}$) is needed. With the knowledge of the frequency and the Cartesian displacement of iron associated with normal modes of the system, the probability density of inelastic nuclear absorption can be calculated.

Calculation of iron vibrational density of states

The experimental measurements on FeTPP(NO) are transformed to yield the iron VDOS. To make a meaningful comparison of our normal-mode calculation with the experimental data, we need to derive the Fe VDOS from the results of our normal-mode analysis. Here we will first describe an expression to calculate the one-phonon contribution to the nuclear absorption probability using the frequencies and the iron amplitudes of the calculated normal modes. The iron VDOS can then be determined directly from the calculated nuclear absorption probability.

The probability of absorption or emission of radiation of wave vector $\mathbf{k}$ by a single nucleus is proportional to the Lamb–Mössbauer factor $f = e^{-\langle \mathbf{k} \cdot \mathbf{u}\rangle^2}$ where $\mathbf{u}$ is the displacement vector for the ^{57}Fe nucleus. The probability density of nuclear absorption of a single ^{57}Fe nucleus in a molecular crystal, such that the vibrational state of the crystal makes a transition from a state $|i\rangle$ to a state $|j\rangle$ is given by (Singwi and Sjölander, 1960; Paulsen et al., 1999),

$$S(E, \hat{k}) = \sum_{i,j} g_i |\langle j|e^{-i\mathbf{k}\cdot\mathbf{u}}|i\rangle|^2 \frac{\Gamma/2\pi}{(E_j - E_i - E)^2 + \Gamma^2/4}, \qquad (3)$$

where g_i is the statistical weight factor for the state $|i\rangle$, E_i and E_j are the energies of the vibrational states $|i\rangle$ and $|j\rangle$, Γ is the linewidth of the vibrational transition, and E is the difference between the energy of the incident radiation and the nuclear resonance energy of ^{57}Fe. The summation over all the vibrational states can be avoided by replacing the Lorentzian by its Fourier transform and by expressing the operator $e^{-i\mathbf{k}\cdot\mathbf{u}}$ of the transition matrix element in the interaction representation as $\langle e^{-i\mathbf{k}\cdot\mathbf{u}(0)} e^{+i\mathbf{k}\cdot\mathbf{u}(t)}\rangle$, as described by Singwi and Sjölander (1960) and by
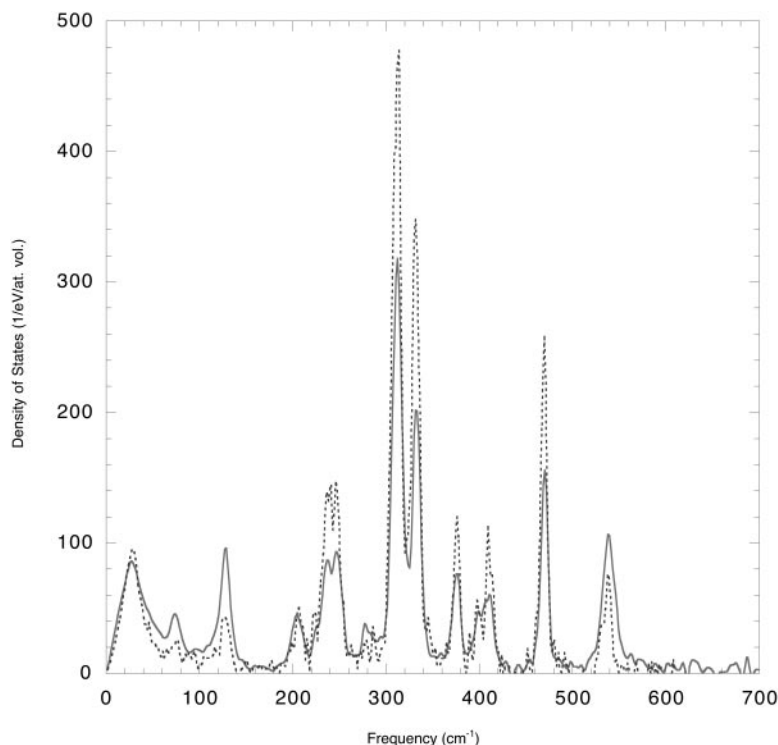
FIGURE 2 Measured NRVS spectra of polycrystalline powder sample (——) and single crystals (- - - -) of FeTPP(NO). The measurements on the polycrystalline powder sample and single crystals were performed at 70 and 20 K, respectively. For the measurements on the single crystals of FeTPP(NO), the incident wave vector, **k**, made an angle of 6° from the heme plane.

Paulsen et al. (1999). Following those authors, the one-phonon contribution to the absorption probability is expressed as (Paulsen et al., 1999)

$$S_1(E, \hat{k}) = e^{-\langle(\mathbf{k}\cdot\mathbf{u})^2\rangle} \sum_{l=1}^{L} e^{\beta E_l/2}$$

$$\times \frac{\Gamma/2\pi}{(E - E_l)^2 + \Gamma^2/4} \prod_{j=1}^{L} I_{n_j}(C_j(\hat{k})), \quad (4)$$

where L is the total number of iron modes, β is $1/kT$ (k is the Boltzmann's constant and T is absolute temperature), and I_{n_j} is the Bessel function of the first kind of order n_j. The value of Γ we set to 8 cm^{-1}, corresponding to the experimental energy resolution. We set $n_j = \delta_{lj}$ because we are calculating the one-phonon absorption probability. The argument $C_j(\hat{k})$ of the Bessel function is defined as

$$C_j(\hat{k}) = \frac{\langle(\mathbf{k} \cdot \mathbf{u}_j)^2\rangle}{\cosh(\beta E_j/2)}. \quad (5)$$

The iron vibrational density of states is directly related to the one-phonon absorption probability (Sturhahn et al., 1995; Singwi and Sjölander, 1960),

$$D(E) = 3 \frac{E}{E_R} \frac{S_1(E)}{f} [1 - e^{-\beta E}], \quad (6)$$

where E_R (= 1.96 meV) is the recoil energy of ^{57}Fe nucleus and f is the Lamb–Mössbauer factor. Using Eq. 6 along with Eqs. 5 and 4, we calculate the Fe VDOS, which is then compared to the experimental iron VDOS.

EXPERIMENTAL RESULTS

NRVS measurements were performed on a polycrystalline sample of FeTPP(NO) at 70 K; the iron VDOS extracted from absorption data is shown in Fig. 2. To distinguish between modes having iron displacement either predominantly parallel or perpendicular to the heme plane, NRVS data were also obtained for a set of oriented single crystals at 20 K. These small single crystals were mounted together on a single flat substrate, each with the normal to the heme planes perpendicular to the surface (with an estimated uncertainty of a few degrees). The NRVS absorption probability depends on the vibrational motion being parallel to the incident x-ray beam. Hence, the VDOS derived from single crystals would not be the same as that from a powder specimen, because any iron motion perpendicular to the x-ray beam would not contribute to the absorption process. This effect is analogous to laboratory Mössbauer absorption spectroscopy, where the sample must be accelerated in the direction of the gamma ray source, producing a Doppler shift of the photon energy. Because these data were obtained with the incident beam at ~6° angle to the heme plane, the resulting absorption spectrum will be significantly weighted toward the in-plane Fe modes. A comparison with the powder spectrum (Fig. 2) thus permits immediate identification of the major in-plane and out-of-plane iron modes.

The iron VDOS for the oriented single crystals of FeTP-P(NO) derived from the measured spectra are shown in Fig. 2. These spectra reveal a total of 14 distinct modes in the energy range of 0–700 cm^{-1}. Except for the lowest frequency mode near 28 cm^{-1}, the observed modes have widths that are essentially limited by instrumental resolution, and show little dispersion.

The comparison of iron VDOS reveals the presence of three modes with suppressed VDOS in the crystal spectrum, indicating that the displacement vector of iron for those modes has a large component perpendicular to the heme plane. One of these is at a high frequency, 538 cm^{-1}, which we shall identify as the FeN$_L$ stretch mode as expected from Raman data (Choi et al., 1991; Lipscomb et al., 1993; Vogel et al., 1999). The remaining two modes are in the low frequency region of the spectrum (at 74 and 128 cm^{-1}), which we find are doming and tilting modes of the heme. In contrast, an increase of ∼50% in the iron VDOS for the crystals with respect to the powdered sample is observed for modes at 313, 333, and 470 cm^{-1}, indicating a strong in-plane character.

COMPUTATIONAL RESULTS AND DISCUSSION

The normal mode analysis of FeTPP(NO) with 79 atoms results in 231 nonzero eigenvalues. In the absence of an axial ligand and with iron atom lying in the heme plane, the system has a symmetry type of D_{4h}. The in-plane vibrations of the 37-atom porphyrin core can be classified as (Spiro and Li, 1988; Procyk and Brocian, 1992), $\Gamma_{ip} = 9A_{1g} + 8A_{2g} + 9B_{1g} + 9B_{2g} + 18E_u$, and the corresponding out-of-plane vibrations are $\Gamma_{op} = 3A_{1g} + 6A_{2u} + 5B_{1u} + 4B_{2u} + 8E_g$. Iron displacement occurs only for E_u and A_{2u} modes; the iron displacement is zero for all other modes. Hence NRVS would only detect E_u and A_{2u} modes for a heme with D_{4h} symmetry. Note that both of these modes are Raman inactive. Although intra-phenyl modes do not directly include any iron motion, the mixing of ligand and phenyl ring vibrations with the porphyrin modes could produce iron displacement detectable with NRVS. A ligand conformation that breaks the D_{4h} symmetry can also produce other observable modes.

Using an initial set of force constants developed for nickel porphyrins (Li et al., 1989; Rush et al., 2000), normal mode calculations of the FeTPP(NO) model yielded a good match to previously reported frequencies of the prominent high-frequency marker lines seen in Raman data (Spiro and Li, 1988). These initial results gave iron VDOS that completely disagreed with the NRVS data, however. This discrepancy is due in part to using nickel force constants instead of those for iron. In addition, the presence of an NO ligand can also lead to changes in the force constants and a lower symmetry, affecting the dynamics of the iron atom.

A refinement of the force field was needed to achieve good agreement between the calculated and experimental

values of the frequency and amplitude for all the observed modes. The refinement procedure was based on the well-known Jacobian Determinant method (Levin and Pearce, 1975). In addition to relying on this computational algorithm, force constants were also adjusted by trial and error to obtain improved fits to the data. Refinement was constrained to keep the frequencies of 10 marker lines, with frequencies between 1200 and 1600 cm^{-1}, near (within ±30 cm^{-1}) their published Raman values. A comparison of the experimental iron VDOS with the best-fit normal mode calculation is shown in Fig. 3. The best-fit values of some force constants having significant influence on the iron vibrational spectrum are shown in Table 2. The final refined values of Fe-N$_{P,I}$ and Fe-N$_{P,III}$ stretch force constants are slightly larger than the best-fit force constants Fe-N$_{P,II}$ and Fe-N$_{P,IV}$. This result is consistent with the previously reported x-ray measurement (Scheidt et al., 2000), where Fe-N$_{P,I}$ and Fe-N$_{P,III}$ have nearly equal bond lengths that are slightly greater than the nearly identical bond lengths of Fe-N$_{P,II}$ and Fe-N$_{P,IV}$. The average value of the best-fit Fe-N$_P$ force constant (1.42 mdyne/Å) is found to be 21% smaller than the Ni-N$_P$ force constant (1.80 mdyne/Å), which was chosen as the initial value for Fe-N$_P$ force constant in our calculation. Similarly, a comparison of N$_{P,X}$-Fe-N$_L$ (X = I, II, III, or IV) bending force constants from Table 2 indicates a structural asymmetry associated with the off-axial tilt of Fe-N$_L$ bond toward the quadrant defined by N$_{P,I}$-Fe-N$_{P,II}$, as evident from the x-ray measurement (Scheidt et al., 2000).

The experimentally observed modes are assigned by characterizing the calculated modes according to the classification scheme developed for D_{4h} symmetric porphyrin (Abe et al., 1978; Spiro and Li, 1988; Procyk and Brocian, 1992). The classification of normal modes according to this scheme is done by first defining pseudo eigenvectors representing the normalized mass-weighted normal coordinates of porphyrin core vibrational modes (ν_1 to ν_{53} and γ_1 to γ_{26}). Then the calculated normal modes are assigned by taking the inner product of the pseudo eigenvectors with all the modes obtained from the calculation. In the case of a calculation performed on a D_{4h} symmetric porphyrin model without any peripheral substituents or axial ligands, we would expect the absolute value of the inner product of a particular pseudo eigenvector (ν_i) with all the calculated eigenvectors to be close to zero for all the modes except one. There would also be one normal-mode eigenvector whose inner product with the pseudo eigenvector (ν_i) to be close to +1 or −1; this normal vibration is then assigned as a ν_i mode. In other words, any given pseudo eigenvector (ν_1 to ν_{53} or γ_1 to γ_{26}) will be orthogonal to all but one normal mode of a four-fold symmetric porphyrin core. However, in the case of FeTPP(NO), which has phenyl substituents and an off-axial NO ligand, a mixing of the porphyrin core modes will occur. Thus, for some pseudo eigenvectors,
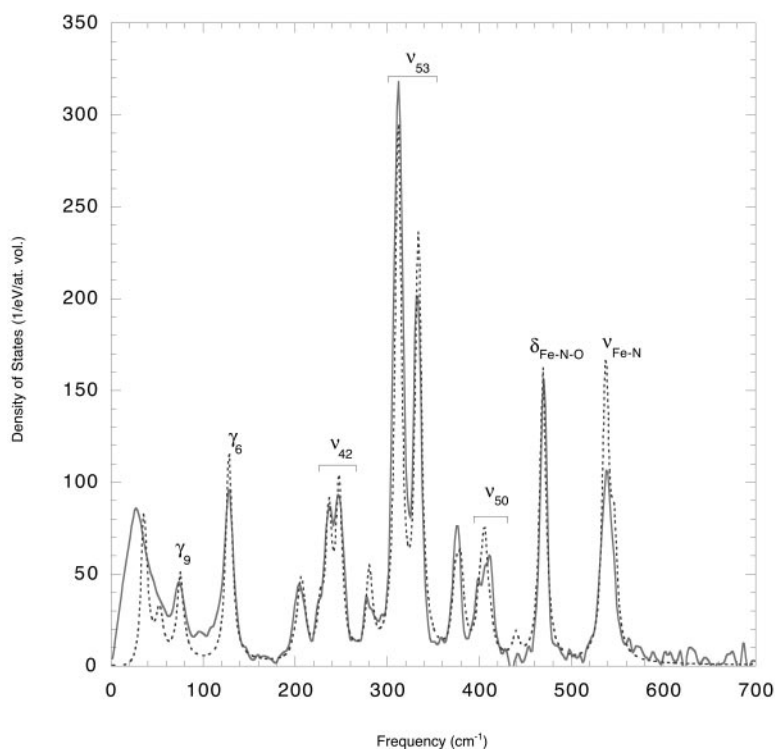
FIGURE 3   The measured (—) and calculated (- - - -) iron vibrational density of states. The calculated VDOS is multiplied by an arbitrary scale factor.

we may have more than one calculated eigenvector whose inner product with it is far from zero. In such cases, the calculated eigenvector having the largest absolute value of inner product with the pseudo eigenvector (v_i) will be assigned as a v_i mode.

Table 3 indicates the extent of overlap for some calculated eigenvectors with the pseudo eigenvectors corresponding to the γ, v, or ligand vibrations. Note that the overlap of any given pseudo eigenvector with the calculated eigenvectors can exceed unity, because the porphyrin pseudo eigenvectors do not form a complete basis set for the eigenvectors of the FeTPP(NO) compound. The calculated mode at 74 cm^{-1}, which we assign as a γ_9 mode, shows a considerable amount of mixing with the ligand and pyrolle tilting (γ_6) vibrations. Similarly, the 128-cm^{-1} mode is significantly mixed with doming and ligand vibrations. Other modes at

higher frequencies also show substantial amount of mixing of porphyrin normal coordinates.

The normal modes are also characterized in terms of their bond stretching, bending, torsion, and out-of-plane bending internal coordinates. Table 4 shows the calculated and observed frequencies of the modes along with their assignments and PED. The PED of a normal mode gives information on the contribution of each force constant F_{ij} of the F matrix (see normal mode analysis) to its potential energy. For a given normal mode, its PED can be calculated by first transforming the mass-weighted Cartesian displacement coordinates ($\mathbf{q}$), as obtained by Eq. 2, into the internal coordinates. The transformation equation can be written as

$$\mathbf{s} = B\mathbf{q}, \quad (7)$$

where B is the transformation matrix as defined in the Normal Mode Analysis section. The length of the vector $\mathbf{s}$ is equal to the total number of internal coordinates (stretch, bend, etc.) used to describe the potential energy of the system. The contribution to the potential energy of a normal mode from the diagonal and off-diagonal elements of the force constant matrix F is given by $\frac{1}{2}F_{ii}s_i^2$ and $\frac{1}{2}F_{ij}s_is_j$, respectively.

The modes can be divided into the following four groups: 1) in-plane modes of the porphyrin core (v_{53}, v_{50}, and v_{42}); 2) ligand modes at 547 (τ_{FeN_L}), 538 (v_{FeN_L}), 470 (δ_{FeN_LO}),

TABLE 2   The best-fit values of some of the force constants having significant influence on iron vibrational spectrum*

Force constant (mdyn/Å)		Force constant (mdyn Å/rad^2)	
Fe-N(I)	1.35	N(I)-Fe-N$_L$	0.91
Fe-N(II)	1.49	N(II)-Fe-N$_L$	0.91
Fe-N(III)	1.35	N(III)-Fe-N$_L$	0.55
Fe-N(IV)	1.49	N(IV)-Fe-N$_L$	0.55
Fe-N$_L$	2.66	Fe-N$_L$-O	0.30

*A complete list of force constants is available from the authors.

TABLE 3 Percentage overlap of various calculated modes with relevant porphyrin core and ligand vibrations

Freq (cm^{-1})	Assignment	γ_9	γ_6	v_{42a}	v_{42b}	v_{53a}	v_{53b}	v_{50a}	v_{50b}	δ_{FeN_LO}	v_{FeN_L}
75	γ_9	39	16	0.2	0.2	3	2	1	1	10	2
128	γ_6	25	28	0.1	0.1	2	2	1	1	34	1
205*	—	5	1	14	1	10	12	9	8	7	1
208*	—	–	–	1	14	13	11	9	11	1	–
237	v_{42a}	8	9	23	2	1	1	19	17	5	2
248	v_{42b}	1	1	1	21	1	1	15	18	3	1
281*	—	4	3	4	2	13	12	10	11	6	6
313	v_{53a}	0.2	3	–	–	25	13	7	2	8	2
333	v_{53b}	9	21	3	1	12	27	3	9	35	2
376*	—	2	1	10	12	4	18	31	7	5	5
400	v_{50a}	2	3	1	1	6	17	36	11	3	1
406	v_{50b}	7	8	2	1	22	10	11	41	2	2
470	δ_{FeN_LO}	35	26	–	–	–	2	5	7	60	3
538	v_{FeN_L}	7	–	12	15	12	12	5	4	30	57
547	—	–	–	8	11	11	11	2	4	21	13

*This mode cannot be assigned as any of the γ, v, or ligand vibrations.
The numbers indicate the scalar product of calculated eigenvectors with the pseudo-eigenvectors corresponding to the γ, v, or ligand vibrations. The calculated scalar products were multiplied by 100 to get the percentage overlap.

and 279 cm^{-1}; 3) modes at 376, 54, 52, and 36 cm^{-1} involving vibrations of the phenyl rings; and 4) out-of-plane modes at 74 (γ_9) and 128 (γ_6) cm^{-1}.

In-plane porphyrin modes v_{53}, v_{50}, and v_{42}

The v_{53}, v_{50}, and v_{42} modes are doubly degenerate in porphyrin compounds having D_{4h} symmetry and are of E_u

symmetry type, which makes them Raman inactive. The presence of an off-axis NO ligand reduces the four-fold symmetry, which lifts the degeneracy of these modes. The removal of D_{4h} symmetry may make these modes Raman active, but they have not yet been unambiguously identified in Raman scattering.

The most striking feature in the iron vibrational density of states (Fig. 2), the doublet at 313 and 333 cm^{-1}, is a v_{53}

TABLE 4 Frequencies of the observed and calculated modes, mode assignments and potential energy distribution

Observed Frequency (cm^{-1})	Calculated Frequency (cm^{-1})	Mode Assignment	PED(%)
27	36	v_{Phenyl} (op)	δ_{FeN_LO} (23)
	52	v_{Phenyl} (ip)	$\delta_{C_\alpha C_{m,I} C_1}$ (19) + $\delta_{C_\alpha C_{m,III} C_3}$ (19) + $\tau_{C_{m,I} C_1 C_{P,I} C_{P,I}}$ (17) + $\tau_{C_{m,I} C_1 C_{P,I} C_{P,I}}$ (17)
	54	v_{Phenyl} (ip)	$\delta_{C_\alpha C_{m,II} C_2}$ (21) + $\delta_{C_\alpha C_{m,IV} C_4}$ (21) + $\tau_{C_{m,II} C_2 C_{P,II} C_{P,II}}$ (15) + $\tau_{C_{m,IV} C_4 C_{P,IV} C_{P,IV}}$ (15)
74	75	γ_9 (op)	$v_{FeN_{P,I}}$ (7) + $\delta_{N_{P,I} FeN_L}$ (7) + $\delta_{N_{P,II} FeN_L}$ (4) + δ_{FeN_LO} (40)
128	128	γ_6 (op)	$\delta_{N_{P,III} FeN_L}$ (19) + $\delta_{N_{P,IV} FeN_L}$ (15) + $\delta_{C_{m,III} C_3 C_{P,III}}$ (5) + $\delta_{C_{m,IV} C_4 C_{P,IV}}$ (10)
205	205	ip	$v_{C_{m,II} C_2}$ (13) + $v_{C_{m,IV} C_4}$ (12)
	208	ip	$v_{C_{m,I} C_1}$ (13) + $v_{C_{m,III} C_3}$ (13)
227	228	ip	δ_{FeN_LO} (6) + $\delta_{C_{m,I} C_1 C_{P,I}}$ (10) + $\delta_{C_{m,II} C_2 C_{P,II}}$ (8) + $\delta_{C_{m,III} C_3 C_{P,III}}$ (9) + $\delta_{C_{m,IV} C_4 C_{P,IV}}$ (13)
237	237	v_{42a} (ip)	$\tau_{C_{m,I} C_1 C_{P,I} C_{P,I}}$ (7) + $\tau_{C_{m,III} C_3 C_{P,III} C_{P,III}}$ (8)
247	248	v_{42b} (ip)	$\tau_{C_{m,II} C_3 C_{P,II} C_{P,II}}$ (12) + $\tau_{C_{m,IV} C_4 C_{P,IV} C_{P,IV}}$ (14) + $\tau_{C_{P,II} C_2 C_{P,II}}$ (6) + $\tau_{C_{P,IV} C_4 C_{P,IV} C_{P,IV}}$ (6)
279	281	ip	$\tau_{FeN_{P,IV}}$ (11) + v_{FeN_L} (4) + $\delta_{FeN_L}O$ (19)
313	312	v_{53a} (ip)	$v_{FeN_{P,I}}$ (17) + $v_{FeN_{P,II}}$ (4) + $v_{FeN_{P,III}}$ (16) + $v_{FeN_{P,IV}}$ (5) + $\delta_{N_{P,II} FeN_{P,II}}$ (6)
333	334	v_{53b} (ip)	$v_{FeN_{P,I}}$ (5) + $v_{FeN_{P,II}}$ (8) + $v_{FeN_{P,IV}}$ (4) + $\delta_{N_{P,I} FeN_{P,II}}$ (5) + $\delta_{N_{P,III} FeN_{P,IV}}$ (4) + δ_{FeN_LO} (6)
376	374	ip	$v_{FeN_{P,I}}$ (14) + $v_{FeN_{P,III}}$ (8) + $\gamma_{C_{P,I} H_{P,I}}$ (7) + $\gamma_{C_{P,II} H_{P,II}}$ (10) + $\gamma_{C_{P,III} H_{P,III}}$ (6) + $\gamma_{C_{P,IV} H_{P,IV}}$ (10)
400	400	v_{50a} (ip)	$v_{FeN_{P,I}}$ (6) + $v_{FeN_{P,III}}$ (8) + $\gamma_{C_{P,II} H_{P,II}}$ (16) + $\gamma_{C_{P,IV}} H_{P,IV}$ (17)
410	406	v_{50b} (ip)	$v_{FeN_{P,II}}$ (13) + $v_{FeN_{P,IV}}$ (11) + $\gamma_{C_{P,I} H_{P,R}}$ (10) + $\gamma_{C_{P,III} H_{P,III}}$ (11)
470	470	δ_{FeN_LO} (op)	$\delta_{FeN_L}O$ (12) + $\delta_{N_{P,I} FeN_L}$ (11) + $\delta_{N_{P,II} FeN_L}$ (8)
538	539	v_{FeN_L} (op)	v_{FeN_L} (41) + $\delta_{FeN_L}O$ (5) + $\delta_{N_P FeN_L}$ (7) + τ_{FeN_L}
547	547	τ_{FeN_L} (ip)	τ_{FeN_L} (45) + $\delta_{N_P FeN_L}$ (16)

The in-plane and out-of-plane motions of iron are indicated by ip and op, respectively. The contribution to the potential energy of a particular normal mode from stretch (v), angle bend (δ), torsion (τ), and out-of-plane bend (γ) force constants is shown. The number in the parentheses indicates the percentage contribution of a given force constant to the PED of the mode. Only those force constants that contribute 4% or more to the PED are listed.
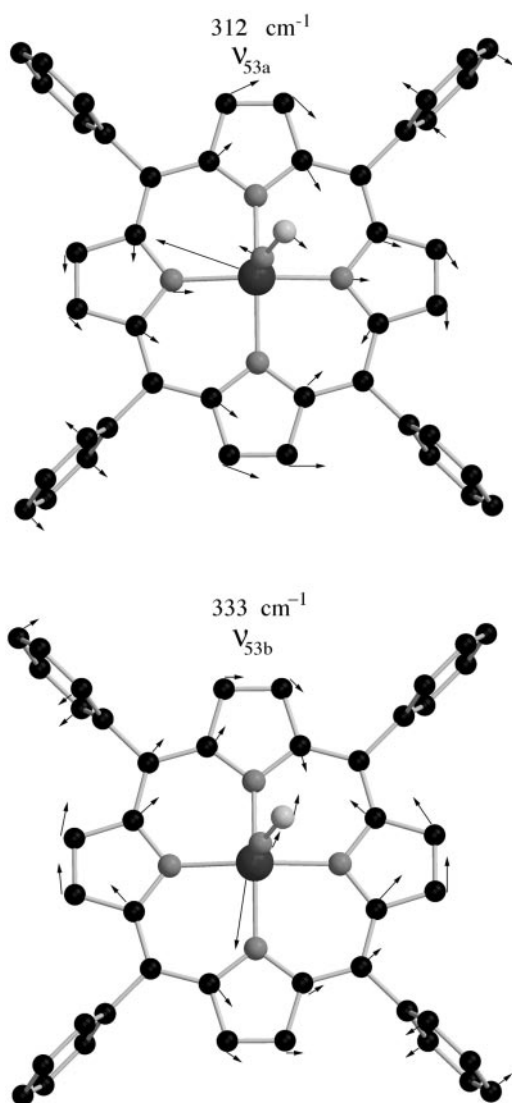
FIGURE 4 The eigenvectors of in-plane v_{53a} and v_{53b} modes. The lengths of the arrows indicate relative magnitudes of atom displacements.

FIGURE 5 The eigenvector of v_{50b} mode at 406 cm^{-1}. The lengths of the arrows indicate relative magnitudes of atom displacements.

mode. The oriented crystal data indicate a large in-plane component of iron atom. The v_{53} mode is characterized by in-plane motion of the two pyrrole rings situated directly opposite to each other, oscillating in-phase and opposed by motion of the iron atom. The iron displacements in the v_{53a} and v_{53b} modes are essentially orthogonal to each other (Fig. 4). The v_{53b} mode is coupled to the FeN$_L$ stretch and FeN$_L$O bend motions, which causes a splitting in the doubly degenerate v_{53} modes and shifting the coupled mode, v_{53b}, to a higher frequency. The m.s.d. of iron for the v_{53b} mode decreases as the whole FeN$_L$O unit now opposes the displacement of pyrrole rings. The PED of these two modes contains large contributions from FeN$_P$ stretch force constants, as shown in Table 4.

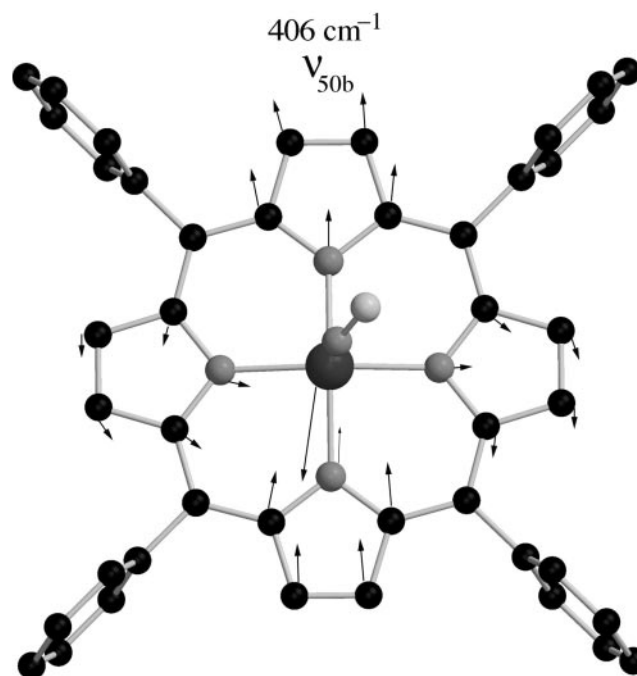The v_{50} mode is defined as an asymmetric Fe-pyrrole stretch. The presence of an off-axis NO ligand removes the two-fold degeneracy, causing two distinct vibrations at 400 and 410 cm^{-1}. The largest contribution to the PED comes from the FeN$_P$ stretch force constants; the character of one of the v_{50} modes (calculated to be at 406 cm^{-1}) is shown in Fig. 5. The v_{42} mode involves an out-of-phase displacement of iron against the two phenyl rings situated diametrically opposite to each other. The two-fold degeneracy of v_{42} mode is also lifted by the off-axis NO ligand, and two closely spaced modes at 237 and 247 cm^{-1} appear in the NRVS spectra for FeTPP(NO). The atomic displacements of the v_{42} mode at 247 cm^{-1} are shown in Fig. 6.

Ligand modes

The experimental mode at frequency 538 cm^{-1} is broader than the instrumental resolution, indicating the presence of two closely-spaced vibrational modes. We assign this feature to be an FeN$_L$ stretch at 538 cm^{-1} plus a torsional motion around the FeN$_L$ bond at 547 cm^{-1}. The potential energy distribution of the v_{FeN}L mode shows a predominant ($\sim$40%) contribution to its PED from the FeN$_L$ stretch force constant, yielding an Fe displacement perpendicular to the heme plane. This is consistent with the single crystal data (Fig. 2).

The FeN$_L$ stretch mode is readily observed with resonant Raman spectroscopy in both five- and six-coordinated heme compounds (Choi et al., 1991; Lipscomb et al., 1993; Vogel et al., 1999; Tomita et al., 1999), because of strong coupling to the Soret $\pi \rightarrow \pi^*$ transition. The v_{FeN_L} mode has been
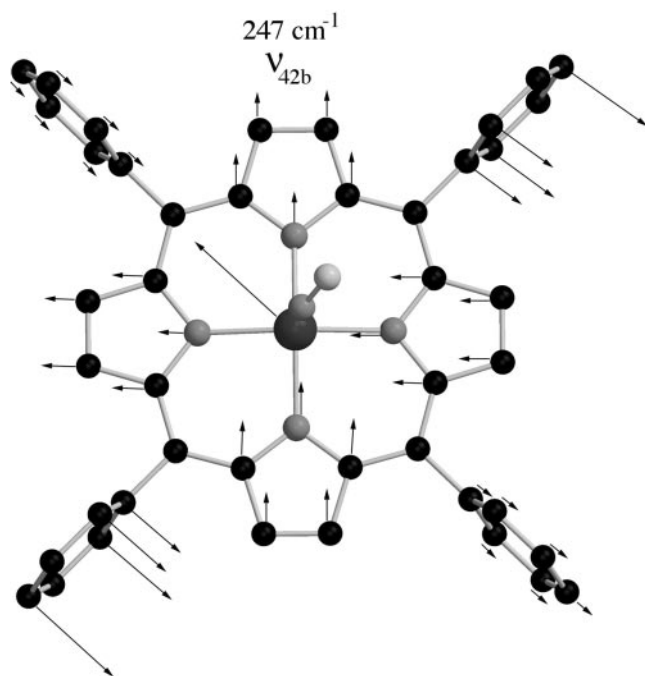
247 cm^{-1}

ν_{42b}

FIGURE 6 The eigenvector of ν_{42b} mode at 247 cm^{-1}. The lengths of the arrows indicate relative magnitudes of atom displacements.

studied to deduce the extent of electron donation from iron to NO. This electron donation increases the bond strength of FeN$_L$ and simultaneously decreases the bond strength of N–O stretch. The FeN$_L$ stretch vibrational frequency is known to be very sensitive to solvents and to protein residues, as well as to the trans-axial ligands. The frequency of FeN$_L$ stretch mode in FeTPP(NO) molecules in the presence of various solvents is typically observed between 515 and 530 cm^{-1}. In the case of our crystalline sample with enriched ^{57}Fe, we observe the ν_{FeNL} mode at a higher frequency of 538 cm^{-1}; this mode is likely to shift upward by an additional 4–6 cm^{-1} in crystals with naturally occurring isotopes of iron. In other words, this mode is 10–20 cm^{-1} higher than expected. Crystal field effects are the most likely cause of this higher frequency shift. A shift of 8 cm^{-1} in the frequency of the FeN$_L$ mode has been detected upon substitution of ^{14}N by ^{15}N in FeTPP(NO) (Vogel et al., 1999). This substitution in our calculation produces a shift of 10 cm^{-1}, indicating a realistic treatment of this mode.

The NRVS crystal data show the mode at 470 cm^{-1} to involve an in-plane displacement of the iron. Our calculation shows this mode to have a $\delta_{\text{FeN}_L\text{O}}$ character, which is mixed with the N$_P$FeN$_L$ tilt and in-plane FeN$_P$ stretch vibrations. Unlike the FeN$_L$ stretch vibration, which is strongly coupled to the Soret $\pi \rightarrow \pi^*$ band, and hence is observed in Raman measurements, the $\delta_{\text{FeN}_L\text{O}}$ mode does not couple to the Soret band and has not been observed in any five-coordinate model heme compound. This mode is

apparently observed, however, in some six-coordinate heme proteins (Tomita et al., 1999). Finally, coupling of the porphyrin ν_{FeN_P} vibration with the ligand bending mode, $\delta_{\text{FeN}_L\text{O}}$, results in a mode at 279 cm^{-1} whose character is very similar to the ν_{53b} mode (section before last) at 333 cm^{-1}.

Phenyl in-plane and out-of-plane modes

The coupling of the phenyl rings with the porphyrin core gives rise to additional features in the NRVS spectrum. The mode at 376 cm^{-1} is attributed to an out-of-plane bending vibration of phenyl hydrogens. Other modes resulting from the coupling of phenyl vibrations with the porphyrin core are found at lower frequencies (below 60 cm^{-1}).

The lowest frequency region of the NRVS spectrum of FeTPP(NO) shows a broad continuous feature. Unlike higher-frequency modes that are resolution limited, this low-frequency band shows a significant amount of dispersion. At low frequency, intermolecular interactions are expected to play an important role. Acoustic modes involving large iron displacements can also be expected. Normal mode calculations for our model FeTPP(NO) were done on a single, isolated molecule, so any crystal effect is neglected. Our calculation shows the presence of three modes in this region, which have large displacement of iron and which may be major contributors to this band. All three of these modes involve large in-phase motion of the phenyl ring atoms. The two modes at 52 and 54 cm^{-1} are quasi-degenerate with orthogonal iron displacements along the heme plane, as shown in Fig. 7. The iron atom moves out-of-phase with the lateral motion of the two diagonally opposite phenyl rings.

The lowest of the three modes in this region shows a large out-of-plane displacement of iron at 37 cm^{-1}. The out-of-plane motion of the iron is opposed by the vertical (out-of-plane) displacement of the four phenyl rings. This mode also shows a coupling to the FeN$_L$O bend and N$_P$FeN$_L$ tilt coordinates, and is shown in Fig. 8. Our calculations determine that these three phenyl modes account for close to 50% of the total m.s.d. of iron. The polarization experiment done on the oriented sample of FeTPP(NO) crystals indicate the presence of both in-plane and out-of-plane modes in the low-frequency region of 0–60 cm^{-1}, in addition to having a significant amount of dispersion. It is therefore likely that this broad, low-frequency feature is a superposition of acoustic and phenyl modes.

Heme out-of-plane γ_9 and γ_6 modes

The heme doming mode is defined in the Fe-porphyrin as an out-of-plane displacement of the iron atom, which is out of phase with the rest of the porphyrin ring atoms (Hoard and
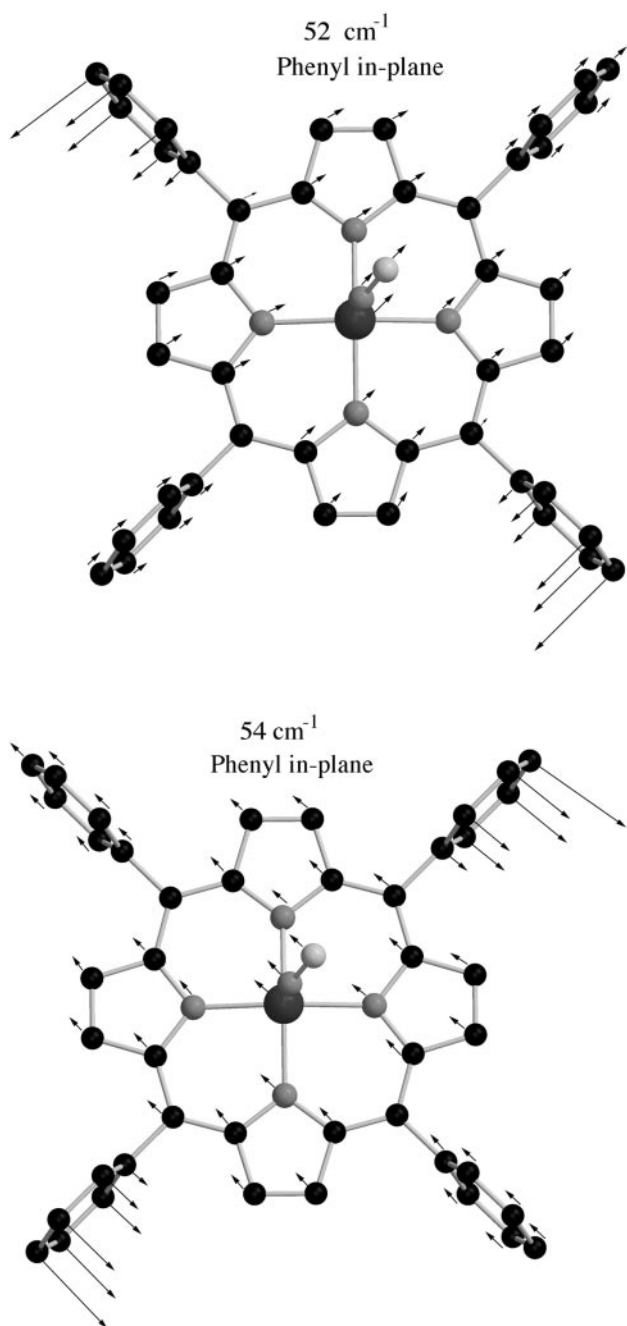
52 cm^{-1}
Phenyl in-plane

54 cm^{-1}
Phenyl in-plane

FIGURE 7 The eigenvectors of quasi-degenerate in-plane modes involving motion phenyl rings at 52 and 54 cm^{-1}. The lengths of the arrows indicate relative magnitudes of atom displacements.

35 cm^{-1}
Phenyl out-of-plane

FIGURE 8 The phenyl out-of-plane mode at 37 cm^{-1}. The number against each atom indicates the relative out-of-plane displacements.

Scheidt, 1973; Perutz, 1970). A knowledge of the frequency and character of modes having doming character is important for heme proteins, where the change in heme doming associated with reversible binding of ligands to the heme iron is propagated to the protein side chains and is believed to trigger the allosteric response in hemoglobin (Hoard and Scheidt, 1973; Perutz, 1970). Despite its importance to the functions of the heme proteins, little direct experimental
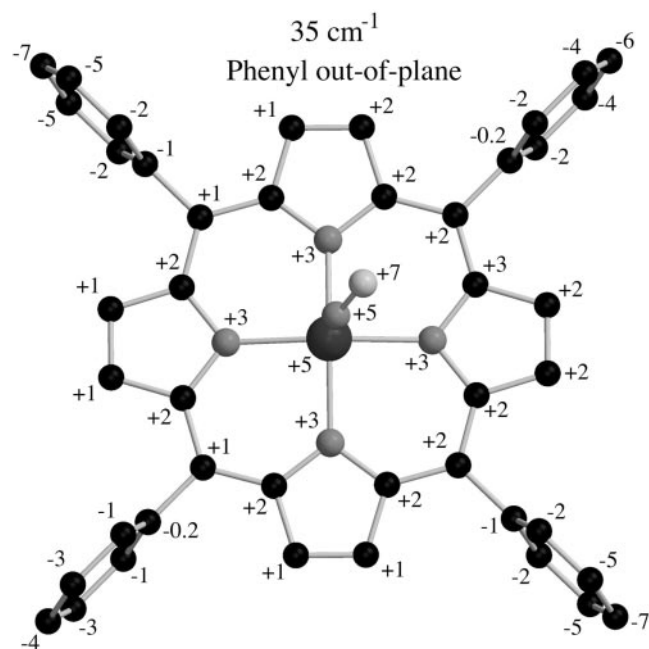
information about doming modes is available. Raman and IR techniques have not been able to directly observe doming modes. In the four-fold symmetric porphyrins, the doming mode is of symmetry type A_{2u}, which is Raman inactive. Although this mode is IR active, its detection is difficult because of a lack of selectivity for iron motions among the large number of protein atoms.

Evidence for a doming mode in myoglobin was observed by Zhu et al. (1994) using femtosecond coherence spectroscopy. In a subsequent study, Rosca et al. (2000) report a low frequency oscillation at 40 cm^{-1} in myoglobin with an NO ligand, which the authors identify as the doming mode. A theoretical study of the doming mode using temperature-dependent data of the iron m.s.d. in myoglobin obtained by conventional Mössbauer technique has been carried out by Li and Zgierski (1992). The iron displacement is harmonic below 165 K. However, above this temperature, the iron motion becomes anharmonic and its m.s.d. increases rapidly with temperature. The anharmonicity in the iron motion has been explained by Li and Zgierski by considering a simple two-state model of a five-coordinated model heme compound; this requires the doming mode to assume two very different values for two different spin states of iron. A normal mode analysis of a four-coordinated model heme compound by the same authors predicts the doming mode to be at 32 cm^{-1}. Their analysis finds the contribution to the total m.s.d. by the doming mode to be 90%. More recent studies by Kozlowski et al. (1998, 2000) on four- and five-coordinated heme models also found the doming mode to be strongly dependent on the spin states of iron. Their

calculated frequencies of the doming mode for different spin states of four- and five-coordinated Iron(II) porphyrins lies between 63 and 98 cm^{-1}.

These discrepancies over the frequency of the doming mode are due in part to a lack of experimental evidence that would allow a confident assignment of the doming mode. NRVS efficiently overcomes the problems associated with Raman and IR measurements, because of its selectivity for iron motion. The effectiveness of this technique to study doming modes is further enhanced by its ability to differentiate between the in-plane and out-of-plane porphyrin modes when using crystalline specimens. Further, the knowledge of iron amplitude in each normal mode allows a better refinement of force fields, resulting in more accurate assignments. Recently, the NRVS technique has been applied to study iron dynamics in deoxy and carboxy myoglobin (Sage et al., 2001a). The lack of a clearly identifiable doming mode in both myoglobins was taken as evidence for a significant delocalization of these modes.

Our NRVS spectrum on the oriented crystals of FeTPP-(NO) shows three normal modes with large out-of-plane iron displacement (Fig. 2). The out-of-plane mode at 538 cm^{-1} has already been identified as the FeN$_L$ stretch mode. The other two out-of-plane modes appear in the low-frequency region at 74 and 128 cm^{-1}. Our normal-mode calculations produce a fit at these frequencies with modes that have large displacements of iron out of the heme plane. The PED of these two modes shows that both modes are highly delocalized, i.e., the potential energy is distributed among a large number of internal coordinates, and they also strongly couple to the N$_P$FeN$_L$ tilt vibrations. The contributions to the PED from the N$_P$FeN$_L$ tilt coordinate are 11% (72 cm^{-1}) and 34% (128 cm^{-1}).

The 72-cm^{-1} mode also has a large (40%) contribution to its PED from FeN$_L$O bending vibrations. For this mode, the vibrations of the ligand are accompanied by a doming-like motion of the porphyrin core (see Fig. 9). The out-of-plane displacement of iron is out-of-phase to the displacement of most of the porphyrin core atoms. Due to a strong coupling of the doming mode with the δ_{FeN_LO} and $\delta_{N_PFeN_L}$ bending vibrations, the frequency of this mode is likely to show a dependence on these force constants. As shown in Table 3, this mode has its greatest overlap with the γ_9 porphyrin doming mode (39%).

The 128-cm^{-1} mode has a 28% overlap with the γ_6 pyrrole tilt mode, and a 25% overlap with the γ_9 doming mode. As shown in Fig. 10, the iron and pyrrole nitrogens move in-phase, accompanied by an out-of-phase displacement of C$_\beta$ atoms. Due to a strong coupling of these modes with the ligand vibrations, it is conceivable that these two modes in myoglobin would act as a pathway of communication between the ligand and the protein side chain. A normal-mode study involving a more realistic model of a heme protein is in progress.
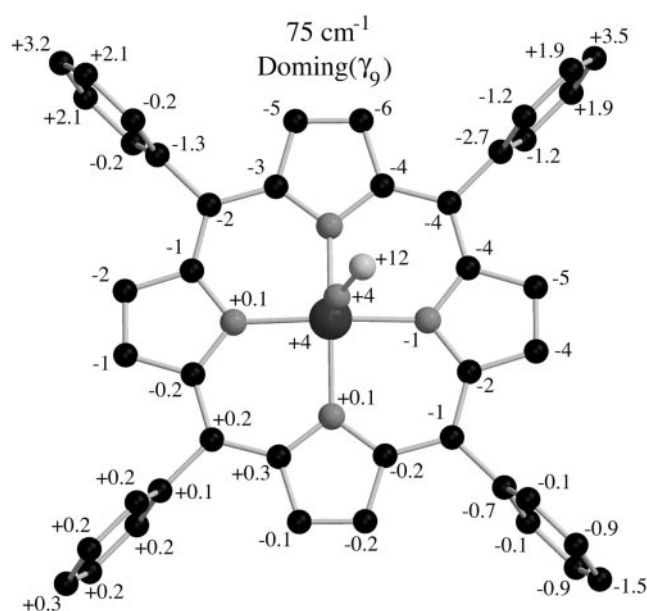

FIGURE 9 The eigenvector of out-of-plane doming (γ_9) mode at 74 cm^{-1}. The number against each atom indicates the direction and relative magnitude of Cartesian displacement vector.

CONCLUSIONS

Iron dynamics in FeTPP(NO) have been studied by NRVS and normal-mode analysis. Measurements on a polycrystalline sample of this compound unambiguously indicate all the vibrational modes involving significant displacement of
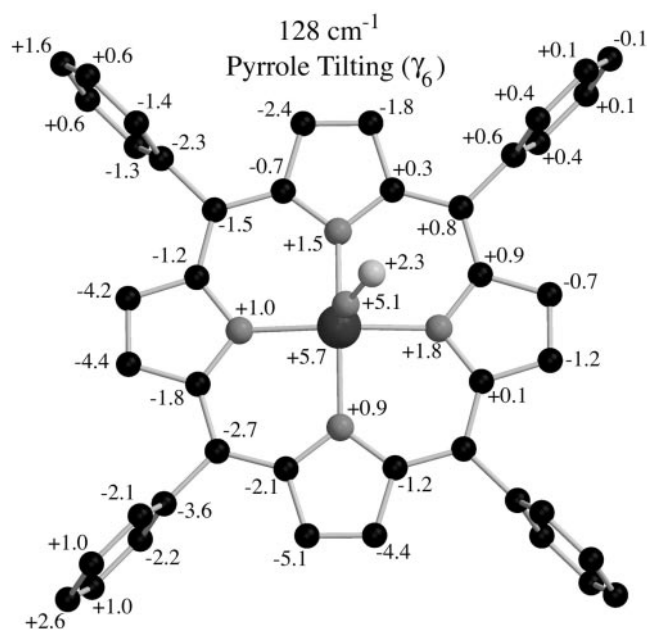

FIGURE 10 The eigenvector of out-of-plane pyrrole tilting (γ_6) mode at 128 cm^{-1}. The number against each atom indicates the direction and relative magnitude of Cartesian displacement vector.

iron. Further insight into iron motion in each vibrational mode is obtained by NRVS measurement on single crystals of FeTPP(NO), which helps in identifying in-plane and out-of-plane vibrations. Good agreement between calculated and measured iron vibrational density of states is achieved by refining the force fields to match the experimental and calculated frequencies and the iron amplitudes. The knowledge of iron m.s.d. obtained by NRVS provides a significant advantage in assigning the observed normal modes. Conventional methods, such as Raman and IR, rely on isotope substitution to make similar assignments, which are often ambiguous because of the delocalized nature of vibrational modes in the low-frequency region of 0–600 cm^{-1}. Furthermore, vibrational selection rules associated with Raman and IR techniques do not allow the detection of a majority of iron modes. In the absence of such selection rules, all iron modes are observed by NRVS. As a result, we have assigned several normal modes that were previously not identified either due to restrictive vibrational selection rules or due to the ambiguity associated with delocalized character of some of the modes. Reduction of four-fold symmetry by the binding of the NO ligand causes the splitting of otherwise doubly degenerate E_u vibrations, which we observe for in-plane modes ν_{53} (313, 333 cm^{-1}), ν_{50} (400, 410 cm^{-1}), and ν_{42} (237, 247 cm^{-1}). In agreement with the previous reports, the ligand stretch (ν_{FeN_t}) mode is observed at 538 cm^{-1}. The mode at 470 cm^{-1} is assigned to the FeN$_L$O bending vibration.

The two out-of-plane modes at 128 and 74 cm^{-1} are found to strongly couple to the ligand vibrations and are highly delocalized in the porphyrin core. The mode at 74 cm^{-1} is assigned to be a doming (γ_9) mode. The character of the 128-cm^{-1} mode involves pyrrole tilting (γ_6) vibrations and significant doming character. The low-frequency features of the VDOS spectrum are due in part to the motion of the peripheral phenyl rings. Acoustic modes are also expected to contribute to the iron VDOS in the low-frequency region. We have demonstrated that one can make confident assignments of iron modes in heme model compounds using NRVS and normal-mode analysis. Building on these results, future studies ought to provide additional insight into iron dynamics in functionally important heme proteins.

REFERENCES

Abe, M., T. Kitagawa, Y. Kyogoku. 1978. Resonance Raman spectra of octaethylporphyrinato-Ni(II) and *meso*-deuterated and ^{15}N substituted derivatives. II. A normal coordinate analysis. *J. Chem. Phys.* 69: 4526–4534.

Choi, I.-K., Y. Liu, D. W. Feng, K.-J. Paeng, and M. D. Ryan. 1991. Electrochemical and spectroscopic studies of iron porphyrin nitrosyls and their reduction products. *Inorg. Chem.* 30:1832–1839.

Chumakov, A. I., and R. Rüffer. 1998. Nuclear inelastic scattering. *Hyperfine Interact.* 113:59–79.

Chumakov, A. I., and W. Sturhahn. 1999. Experimental aspects of inelastic nuclear resonance scattering. *Hyperfine Interact.* 123:781–808.

Cyvin, S. J. 1968. Molecular Vibrations and Mean Square Amplitudes. Elsevier, Amsterdam. 74–79.

Hoard, J. L., and W. R. Scheidt. 1973. Stereochemical trigger for initiating cooperative interaction of the subunits during the oxygenation of Cobaltohemoglobin. *Proc. Natl. Acad. Sci. U.S.A.* 70:3919–3922.

Keppler C., K. Achterhold, A. Ostermann, U. van Bürck, A. I. Chumakov, R. Rüffer, W. Sturhahn, E. E. Alp, and F. G. Parak. 2000. Nuclear forward scattering of synchrotron radiation by deoxymyoglobin. *Eur. Biophys. J. Biophys.* 29:146–152.

Keppler, C., K. Achterhold, A. Ostermann, U. van Bürck, W. Potzel, A. I. Chumakov, A. Q. R. Baron, R. Rüffer, and F. Parak. 1997. Determination of phonon spectrum of iron in myoglobin using inelastic X-ray scattering synchrotron radiation. *Eur. Biophys. J. Biophys.* 25:221–224.

Kincaid, J. R. 2000. Resonance Raman spectra of heme proteins and model compounds. *In* The Porphyrin Handbook. K. M. Kadish, K. M. Smith, and R. Guilard, editors. Vol. 7. Academic Press, New York. 225–291.

Kozlowski, P. M., T. G. Spiro, A. Bérces, and M. Z. Zgierski. 1998. Low-lying spin states of Iron(II) porphine. *J. Phys. Chem. B.* 102: 2603–2608.

Kozlowski, P. M., T. G. Spiro, and M. Z. Zgierski. 2000. DFT study of structure and vibrations in low-lying spin states of five-coordinated deoxyheme model. *J. Phys. Chem. B.* 114:10659–10666.

Landergren, M., and L. Baltzer. 1990. Convenient small-scale method for the insertion of iron into porphyrins. *Inorg. Chem.* 29:556–557.

Levin, I. W., and R. A. R. Pearce. 1975. Intramolecular force field calculations: methods and applications. *In* Vibrational Spectra and Structure. J. R. Durig, editor. Chap. 4. Elsevier, Amsterdam. 102–186.

Li, X.-Y., R. S. Czernuszewicz, J. R. Kincaid, and T. G. Spiro. 1989. Consistent porphyrin force field. 3. Out-of-plane modes in the resonance Raman spectra of planar and ruffled nickel octaethylporphyrin. *J. Am. Chem. Soc.* 111:7012–7023.

Li, X.-Y., R. S. Czernuszewicz, J. R. Kincaid, Y. O. Su, and T. G. Spiro. 1990a. Consistent porphyrin force field. 1. Normal-mode analysis for nickel porphine and nickel tetraphenylporphine from resonance Raman and infrared spectra and isotope shifts. *J. Phys. Chem.* 94:31–47.

Li, X.-Y., R. S. Czernuszewicz, J. R. Kincaid, P. Stein, and T. G. Spiro. 1990b. Consistent porphyrin force field. 2. Nickel octaethylporphyrin skeleta and substituent mode assignments from ^{15}N, meso-d_4, and methylene-d_{16} Raman and infrared isotope shifts. *J. Phys. Chem.* 94:47–61.

Li, X.-Y., and M. Z. Zgierski. 1992. Iron motion in a five-coordinated heme model. *Chem. Phys. Lett.* 188:16–20.

Lipscomb, L. A., B.-S. Lee, and N.-T. Yu. 1993. Resonance Raman investigation of nitric oxide binding in iron porphyrins: detection of the Fe-NO stretching vibration. *Inorg. Chem.* 32:281–286.

Parak, F., and K. Achterhold. 1999. Protein dynamics studied on myoglobin. *Hyperfine Interact.* 123:825–840.

Paulsen, H., H. Winkler, A. X. Trautwein, H. Grünsteudel, V. Rusanov, and H. Toftlund. 1999. Measurement and simulation of nucler inelastic-scattering spectra of moleculear crystals. *Phys. Rev. B.* 59:975–984.

Perutz, M. 1970. Stereochemistry of cooperative effects in hemoglobin. *Nature.* 228:726–739.

Procyk, A. D., and D. F. Bocian. 1992. Vibrational characteristics of tetrapyrrolic macrocycles. *Annu. Rev. Phys. Chem.* 43:465–496.

Rosca, F., A. T. N. Kumar, X. Ye, T. Sjodin, A. A. Demidov, and P. M. Champion. 2000. Investigation of coherent vibrational oscillations in myoglobin. *J. Phys. Chem. A.* 104:4280–4290.

Rush, T. S. III, P. M. Kozlowski, C. A. Piffat, R. Kumble, M. Z. Zgierski, and T. G. Spiro. 2000. Computational modeling of metalloporphyrin structure and vibrational spectra: porphyrin ruffling in NiTPP. *J. Phys. Chem. B.* 104:5020–5034.

Sage, J. T., S. M. Durbin, W. Sturhahn, D. C. Wharton, P. M. Champion, P. Hession, J. Sutter, and E. E. Alp. 2001a. Long-range reactive dynamics in myoglobin. *Phys. Rev. Lett.* 113:4966–4969.

Sage, J. T., C. Paxson, G. R. A. Wyllie, W. Sturhahn, S. M. Durbin, P. M. Champion, E. E. Alp, and W. R. Scheidt. 2001b. Nuclear resonance vibrational spectroscopy of a protein active-site mimic. *J. Phys. Condens. Matter* 13:7707–7722.

Scheidt, W. R., and M. E. Frisse. 1975. Nitrosylmetalloporphyrins. II. Synthesis and molecular stereochemistry of nitrosyl-alpha,beta,gamma,delta-tetraphenylporphyrin(II). *J. Am. Chem. Soc.* 97:17–21.

Scheidt, W. R., H. F. Duval, T. J. Neal, and M. K. Ellison. 2000. Intrinsic structural distortions in five-coordinate (nitrosyl)iron(II) porphyrinate derivatives. *J. Am. Chem. Soc.* 122:4651–4659.

Seto, M., Y. Yoda, S. Kikuta, X. W. Zhang, and M. Ando. 1995. Observation of nuclear resonant scattering accompanied by phonon excitation using synchrotron-radiation. *Phys. Rev. Lett.* 74:3828–3831.

Singwi, K. S, and A. Sjölander. 1960. Resonance absorption of nuclear gamma rays and the dynamics of atomic motions. *Phys. Rev.* 120:1093–1094.

Spiro, T. G., and X.-Y. Li. 1988. Resonance Raman spectroscopy of metalloporphyrins. *In* Biological Applications of Raman Spectroscopy. T. G. Spiro, editor. Chap. 2. Wiley-Interscience, New York. 1–37.

Sturhahn, W. 2000. CONUSS and PHOENIX: evaluation of nuclear resonant scattering data. *Hyperfine Interact.* 125:149–172.

Sturhahn, W., and V. G. Kohn. 1999. Theoretical aspects of incoherent nuclear resonant scattering. *Hyperfine Interact.* 123:367–399.

Sturhahn, W., T. S. Toellner, E. E. Alp, X. Zhang, and M. Ando. 1995. Phonon density-of-states measured by inelastic nuclear resonant scattering. *Phys. Rev. Lett.* 74:3832–3835.

Toellner, T. S., M. Y. Hu, W. Sturhahn, K. Quast, and E. E. Alp. 1997. Inelastic nuclear resonant scattering with sub-meV energy resolution. *Appl. Phys. Lett.* 71:2112–2114.

Tomita, T., S. Hirota, T. Ogura, J. S. Olson, and T. Kitagawa. 1999. Resonance Raman investigation of the FeNO structure of nitrosyl heme in myoglobin and its mutants. *J. Phys. Chem. B.* 103:7044–7054.

Vogel, K. M., P. M. Kozlowski, M. Z. Zgierski, and T. G. Spiro. 1999. Determinants of the FeXO (X = C, N, O) vibrational frequencies in heme adducts from experiment and density functional theory. *J. Am. Chem. Soc.* 121:9915–9921.

Wilson, E. B., J. C. Decius, and P. C. Cross. 1955. Molecular Vibrations. McGraw-Hill, New York.

Zhu, L., P. Li, M. Huang, J. T. Sage, and P. M. Champion. 1994. Real-time observation of low-frequency heme protein vibrations using femtosecond coherence spectroscopy. *Phys. Rev. Lett.* 72:301–304.